

A spectral optimally interpolated mean sea surface from satellite radar altimetry

R. A. Cullen¹ (✉), P. Moore²

¹ Department of Space and Climate Physics, Mullard Space Science Laboratory, Dorking, Surrey RH5 6NT, UK
e-mail: rc@mssl.ucl.ac.uk; Tel.: +44 (0)1483 204163; Fax: +44 (0)1483 278312

² Department of Geomatics, University of Newcastle-upon-Tyne, Newcastle NE1 7RU, UK

Received: 22 December 1999 / Accepted: 6 November 2000

Abstract. A technique is presented for the development of a high-precision and high-resolution mean sea surface model utilising radar altimetric sea surface heights extracted from the geodetic phase of the European Space Agency (ESA) ERS-1 mission. The methodology uses a cubic-spline fit of dual ERS-1 and TOPEX crossovers for the minimisation of radial orbit error. Fourier domain processing techniques are used for spectral optimal interpolation of the mean sea surface in order to reduce residual errors within the initial model. The EGM96 gravity field and sea surface topography models are used as reference fields as part of the determination of spectral components required for the optimal interpolation algorithm. A comparison between the final model and 10 cycles of TOPEX sea surface heights shows differences of between 12.3 and 13.8 cm root mean square (RMS). An un-optimally interpolated surface comparison with TOPEX data gave differences of between 15.7 and 16.2 cm RMS. The methodology results in an approximately 10-cm improvement in accuracy. Further improvement will be attained with the inclusion of stacked altimetry from both current and future missions.

Key words: Mean Sea Surface – Altimetry – FFT

1 Introduction

The accurate determination of the global mean sea surface (MSS) is an important goal in both oceanographic and geodetic studies. It may be defined as a measure of the global average of sea surface heights (SSHs) taken over a period of time suitable to average out annual, semi-annual and other effects. SSHs are best obtained from the spaceborne radar altimeter. Altimetry is unrivalled in the spatial and temporal domains and has an accuracy which is suitable, although in need of improvement.

The resultant surface is a combination of the marine geoid height above a reference ellipsoid, the large-scale mean dynamic ocean topography (sea surface topography), the mean wind and thermohaline circulation-driven dynamic sea surface variability and finally any averaged signal noise. The product's main usage for oceanographic purposes is as a reference surface on which to base computations of variability and large-scale dynamic ocean circulation and for data editing. Of equal importance is its use within geodesy. Although the altimetrically determined gravity anomaly field has received considerable scientific publicity (see e.g. Dickey et al. 1998), it is really only for the measurement of small-scale tectonic signatures of wavelengths less than 200 km. Usage for medium- and long-wavelength studies is limited by fall-off in signal amplitude as a function of increasing wavelength. The mean sea surface, however, contains all global wavelengths including relatively lower-amplitude, short-wavelength signals. Hence, although contaminated with ocean signal, an approximation to the marine geoid may be obtained. Studies such as that of Cazenave et al. (1995) have used the marine geoid from SSHs to infer lithospheric ageing over the Pacific Ocean. Improving the separation of the marine geoid from the dynamic sea surface topography remains an important goal.

In recent years the determination of accurate global high-resolution mean sea surface models has been made possible following the launch of a number of remote sensing satellites with onboard radar altimeters. The combination of TOPEX's (1992–) unrivalled accuracy with the resolution capabilities of ERS-1 (1991–1996) (in particular, its geodetic phase undertaken during 1994/1995), has provided sea surface height measurements at an accuracy and resolution to enable significant improvements over earlier models. With the prospect of additional altimeter missions [GFO (1998–), EnviSat-1 (2001), JASON-1 (2001) and CryoSat (2003)], further refinement of mean sea surface models is expected.

A host of methods are now available to the scientific community for MSS determination both on a regional and on a global scale. For example, methods published

since 1990 have been reported by, amongst others, Blanc et al. (1990), Kim (1993), Rapp et al. (1994), Anzenhofer and Gruber (1995), Yi (1995), Cazenave et al. (1996), Jolly and Moore (1996), Peacock (1998), Knudsen (1999) and Wang (2000). We see a convergence of the accuracy of models for those containing stacked TOPEX, ERS-1/2 and geodetic phase ERS-1 altimetry to about 9.5 cm root mean square (RMS) (see Rapp and Nerem 1995) when compared to TOPEX sea surface heights.

A simple MSS model may be achieved by binning SSHs over a period of a few years and averaging each bin. However, the goal of optimal refinement provides the motivation for continued studies but proves more difficult as various signal errors need to be taken into account. MSS determination from satellite altimetry poses a problem in that each measurement of the ocean surface height contains the marine geoid, sea surface topography, tidal phenomena and a range of errors relating to the measurement itself. Additionally, the measurement is also contaminated by a range of instrumental and environmental measurement errors (discussed in Sect. 3). These can be corrected to a high degree via the use of model corrections or corrections derived from in-situ measurements. There are, however, a number of errors where improvement in model corrections are necessary; these will also be discussed later.

In general, most solutions to the problem of MSS model error minimisation have been restricted to the spatial domain. This has not been a problem to date as results have proven favourable. However, whether improved accuracy can be attributed to the methodology used or to the vast increase and enhancement of measurements is unknown. Nevertheless, each method has its advantages/disadvantages and new approaches are also required in order for improvements to be made. Since the use of spectral domain techniques has proven valuable in geodetic/oceanographic analyses, it was envisaged that MSS model refinement could be possible by the same procedure.

This study takes spatial optimal interpolation as a starting point (see Moritz 1980; Wunsch and Zlotnicki 1984) and develops it for Fourier interpretation. The theory is then applied to the determination of a global high-resolution MSS from ERS-1 satellite altimetry collected during its geodetic phase. A notable advantage of the technique is the speed of computation; however, its main asset is the ability to analyse signals within the Fourier domain.

The model presented has been validated against SSHs derived using independent data from the GEOSAT and TOPEX missions. A comparison is also provided against the original ERS-1 SSHs from which the model was derived. A rigorous analysis of the formal errors within the final surface has been left for future study.

2 Spectral optimal interpolation

Optimal estimation studies of the geoid and MSS have been investigated by Moritz (1980), Wunsch and

Zlotnicki (1984), Blanc et al. (1990), and more recently Jolly and Moore (1996). In this study, spatial optimal interpolation theory is developed from the above references and then transformed to the Fourier domain.

We intend to develop an estimate, \hat{s} , of an unknown signal, s , from a noisy set of observations, l . This estimate is deemed optimum by minimising the least-squares (LS) difference $\langle |\hat{s} - s|^2 \rangle$, where the brackets represent a weighted integral over the surface. In matrix notation the linear estimate, \hat{s} , based on a minimum linear variance, is given by Moritz (1980) as

$$\hat{s} = \mathbf{C}_{sl} \mathbf{C}_{ll}^{-1} \mathbf{l} = \mathbf{a}_{sl} \mathbf{l} \quad (1)$$

where \mathbf{C}_{ll} is the auto-covariance (ACV) function of l and \mathbf{C}_{sl} , the cross-covariance between s and l . Also the parameter, $\mathbf{a}_{sl} = \mathbf{C}_{sl} \mathbf{C}_{ll}^{-1}$ is known as the LS estimator matrix. Now, we make the assumption that the noisy signal, l , is a linear combination of signal, s , and collective noise, n , i.e. $l = s + n$. We find that $\mathbf{C}_{ll} = \mathbf{C}_{ss} + \mathbf{C}_{nn}$ and $\mathbf{C}_{sl} = \mathbf{C}_{ss} + \mathbf{C}_{sn} = \mathbf{C}_{ss}$, where \mathbf{C}_{ss} is the ACV of s , since we assume there is no correlation between signal and noise, i.e. $\mathbf{C}_{sn} = 0$. Hence, Eq. (1) can now be rearranged to give

$$\hat{s} = \mathbf{a}_{sl} \mathbf{l} = \mathbf{C}_{ss} [\mathbf{C}_{ss} + \mathbf{C}_{nn}]^{-1} \mathbf{l} \quad (2)$$

Given the error vector, $\epsilon = \hat{s} - s$, the a posteriori error estimate is given by

$$\mathbf{C}_{\epsilon\epsilon} = \mathbf{C}_{ss} - \mathbf{C}_{ss} [\mathbf{C}_{ss} + \mathbf{C}_{nn}]^{-1} \mathbf{C}_{ss} \quad (3)$$

Our overall intention is to develop a spectral equivalence of Eqs. (2) and (3). Rearranging Eq. 2 we obtain

$$[\mathbf{C}_{ss} + \mathbf{C}_{nn}] \mathbf{a}_{sl} = \mathbf{C}_{ss} \quad (4)$$

The Fourier transform of Eq. (4) is now computed. Note that for two arbitrary signals f and g the power spectral density (PSD) relationship, P_{fg} , is given by

$$P_{fg} = \mathcal{F} \{ C_{fg} - \mu_f \mu_g \} \quad (5)$$

where \mathcal{F} , represents the Fourier operator, whilst μ_f and μ_g are the signal means. If either μ_f or μ_g is zero then

$$P_{fg} = \mathcal{F} \{ C_{fg} \} \quad (6)$$

Substituting $s = f = g$ and $n = f = g$ into Eq. (6) gives Fourier transform pairs, $\mathbf{C}_{ss} \leftrightarrow P_{ss}$, $\mathbf{C}_{nn} \leftrightarrow P_{nn}$ and $\mathbf{a}_{sl} \leftrightarrow A_{sl}$. Since Eq. (4) may be written as a convolution integral in the spatial domain (see e.g. Schwarz et al. 1990), its spectral equivalence is a multiplication of components. Thus

$$[P_{ss} + P_{nn}] A_{sl} = P_{ss} \quad (7)$$

Rearranging Eq. (7) to obtain the spectral LS estimator we obtain

$$A_{sl} = \frac{P_{ss}}{P_{ss} + P_{nn}} \quad (8)$$

Therefore, in the spectral domain the matrix inversion of $[\mathbf{C}_{ss} + \mathbf{C}_{nn}]$ in Eq. (2) is now simply a division of PSDs, P_{ss} and $P_{ss} + P_{nn}$, at each discrete frequency. Transforming Eq. (1) into the spectral domain with $\mathbf{L} \iff L$ and $\hat{\mathbf{s}} \iff \hat{S}$ gives

$$\hat{S} = A_{sl}L = \frac{P_{ss}}{P_{ss} + P_{nn}}L \quad (9)$$

where \hat{S} is the spectral estimation of the MSS, L is the spectrum of the original noisy data set, and A_{sl} is the spectrum of the LS estimator. A_{sl} has been expanded utilising PSDs for P_{ss} , the estimate of signal power, and P_{nn} , the estimate of altimetric measurement noise power in the frequency domain. The inverse of \hat{S} is

$$\hat{s} = \mathcal{F}^{-1} \left[\frac{P_{ss}}{P_{ss} + P_{nn}} L \right] \quad (10)$$

where \mathcal{F}^{-1} denotes the inverse Fourier transform. Thus, A_{sl} is simply a filtering function of the data function l . Also, note that zero noise components within the signal (i.e. $P_{nn} = 0$) will give exact signal replication since $A_{sl} = 1$, i.e. $\hat{S} = L$ or $\hat{s} = l$. Similarly, the a posteriori error covariance estimate of Eq. (3) is modified to

$$\mathbf{C}_{ee} = \mathcal{F}^{-1} \left[P_{ss} - \frac{P_{ss}}{P_{ss} + P_{nn}} P_{ss} \right] \quad (11)$$

P_{nn} within Eqs. (9)–(11) can be developed by a covariance analysis of the noise elements within the data, \mathbf{C}_{nn} . Alternatively, a noise surface may be developed from the altimetry itself, as will be described in Sect. 5.

The fast Fourier transform (FFT) is to be used to put the spectral optimal interpolation into practice and this requires modifications to Eq. (9). There are three main reasons for adapting Eq. (9).

- (1) ERS-1 covers a latitudinal range of $\pm 82^\circ$. Therefore the first MSS guess will contain wavelengths (from the total loss of 16° of information over both polar caps) in the latitudinal direction that cannot be resolved by the FFT.
- (2) Due to the non-periodicity of the surface in the latitudinal direction a windowing procedure is required to smooth SSHs over the latitudinal extremes ($-82^\circ \geq \phi \geq -66^\circ$ and $+66^\circ \leq \phi \leq +82^\circ$). This also results in long-wavelength components being unresolved.
- (3) Finally, it has been suggested (see Wunsch and Zlotnicki 1984) that the spatial LS procedure is improved when a long-wavelength model has been removed. This is based on the premise that reduced power allows an easier distinction between residual signal and noise. It was therefore decided that this methodology should also be applied in the frequency domain.

The procedural modification that is required due to the above three points is the same. That is, the removal of a model geoid to degree and order 30 (cosine tapered to degree 40) and sea surface topography to degree 20, since the latter is only resolvable from the geoid to n

equal to approximately 20 degrees (Tapley et al. 1996). Cosine tapering of the gravity model coefficients is used to reduce spectral ringing [see Cazenave (1994) for a description and example of this phenomenon in terms of spherical harmonic expansions]. Long-wavelength components of the geoid and sea surface topography are re-applied at the end of the procedure.

Following Blanc et al. (1990), the optimal MSS estimate, \hat{h} , at a location with geodetic coordinates (ϕ, λ) is given in the spatial domain by

$$\hat{h}(\phi, \lambda) = h_{lw} + C_{h_0 h_0} [C_{h_0 h_0} + C_{nn}]^{-1} (d_0 - h_{lw}) \quad (12)$$

where \hat{h} is our gridded final optimal estimate; d_0 is the gridded altimetric data set following data editing/geophysical correction (d_0 is the subject of Sect. 3); and h_0 represents an initial guess MSS signature minus a long-wavelength geoid model h_{lw} (i.e. $h_0 = d_0 - h_{lw}$). In this study h_{lw} is the sum of N_{30} , a 30×30 geoid, and ζ_{20} , a 20×20 sea surface topography, both derived from the EGM96 gravity field model (Lemoine et al. 1996), i.e.

$$h_{lw}(\phi, \lambda) = N_{30}(\phi, \lambda) + \zeta_{20}(\phi, \lambda) \quad (13)$$

h_{lw} is removed from the gridded noisy SSHs, d_0 , for reasons described above regarding longer wavelengths being non-resolvable. Also, there are two auto-covariance matrices, namely, $C_{h_0 h_0}$, describing our initial estimate, h_0 , and C_{nn} , the errors within the altimetric signal. Conversion to the spectral domain gives

$$\hat{h} = \mathcal{F}^{-1} \left[H_{lw} + \left(\frac{P_{h_0 h_0}}{P_{h_0 h_0} + P_{nn}} \right) (D_0 - H_{lw}) \right] \quad (14)$$

Equation (14) forms the basis for determining a MSS model in the fast Fourier domain.

3 Altimetry preprocessing

The choice of sea surface measurements was based on the need for optimum high accuracy and resolution. Although the geodetic mission of the US Navy's satellite GEOSAT has the best spatial ground-track resolution to date (4 km at the equator), the geodetic phase of the ERS-1 mission has by far the better accuracy and resolution trade-off. GEOSAT's poor orbital performance, surface tracking ability and lack of on-board microwave radiometer has given it an inferior overall performance with respect to ERS-1. The ERS-1 geodetic phase commenced on 10 April 1994 and ended on 23 March 1995. It consisted of approximately two cycles of 168 days with a total of 2411 arcs per cycle. An orbital manoeuvre at the end of the first cycle allowed the ground tracks of the two cycles to interleave and attain an improvement in the 168-day repeat ground-track resolution by a factor 2. Thus, the resultant equatorial ground-track spacing is approximately 8 km. The immediate release of the geodetic ERS-1 global altimetry eclipsed that of GEOSAT and resulted in the first high-resolution and high-accuracy maps of the geoid and mean sea surface (see Cazenave et al. 1996).

Off-line Ocean Product (OPR) data (CERSAT, 1994) for the entire ERS-1 geodetic phase for Modified Julian Dates (MJD), MJDs 49,454–49,790 (10 April 1994 to 23 March 1995) have been used. The altimetric geophysical data records (GDR) were edited for land/ice flagged data, leaving only ocean/shallow SSHs. Inclusion of shallow sea data supplies optimum data, despite the poor tidal definition over the majority of shallow water and coastal regions.

Altimetry is subject to a number of measurement inadequacies due to imprecise knowledge of the satellite location, effects of the environment on electromagnetic radar energy and the instrument performance itself. Of these, the major error aliased into SSHs is the radial orbit error. Radial height mis-modelling is attributed to errors within the gravitational field, mis-modelling of atmospheric drag and sparsity in tracking of the satellite. ERS-1 suffered the failure of the precise range and range rate equipment (PRARE) shortly after launch, leaving satellite laser ranging and the altimeter itself as the sole tracking systems. However, an alternative means of orbit enhancement is provided by dual-satellite crossover residuals with TOPEX/Poseidon (T/P). Dual-satellite crossover analysis (Carnochan et al. 1994), as used to minimise orbital error, works on the principle that a satellite (T/P) with accurate ephemeris may be used to correct another (ERS-1) with less accurate ephemeris.

T/P was launched into an orbital altitude of approximately 1336 km with lower atmospheric drag and gravitational attraction than ERS-1. T/P also has superior tracking from DORIS and global positioning systems (GPS) yielding better-determined orbits. Fortunately, both platforms were operational during the majority of the ERS-1 mission apart from the early commissioning and ice phases and the first five cycles of the first multidisciplinary phase. Ground-track crossovers, with epochs differing by 5 days or less in order to reduce any long-term oceanic variability, yield discrete corrections to the orbit of ERS-1.

TOPEX–ERS-1 (T/P–E) crossover residuals were computed at all crossover locations from T/P SSHs corrected for all environmental effects as specified by AVISO (1996). An initial removal of a 44-cm bias was performed and erroneous residuals rejected with a threshold of 1 m. Residuals were then split into TOPEX–ERS-1 (T–E) and Poseidon–ERS-1 (P–E) sets. An additional bias was computed for each set and a $3\text{-}\sigma$ rejection criterion applied. The dual crossover data yielded a total of 460 120 residuals with RMS crossover differences of 12.11 and 11.39 cm between ERS-1, TOPEX and ERS-1, Poseidon respectively.

A continuous orbit error correction was computed using a B -spline fit to dual ERS-1 and TOPEX crossovers using a modified Le Traon et al. (1995) method (see Cullen 1998 for further details). There are two principle differences between the method adopted here and that of Le Traon et al. (1995). First, as the number of crossovers per unit area is latitudinally dependent, it is advisable to introduce a higher significance to equatorially based crossovers. Hence the i th residual was

weighted as a function of latitude, ϕ , through $W_i = \cos^2 \phi_i$. The second difference between the methods was the exclusion of single ERS-1 crossovers. Single ERS-1 crossovers both outside the ($> |66^\circ|$) latitudinal coverage of TOPEX and in coastal/continental shelf regions constrain (although complicate) the cubic fitting procedure but have been shown to reduce the orbit error in these regions. However, inclusion of these crossovers in the procedure was relaxed as these regions suffer from poor tidal modelling with high latitudes being subject to windowing for spectral processing. Thus, the final product was set to cover the latitudes within the range of TOPEX.

The overall reduction in radial orbit error stems from the cubic spline fit to high-amplitude long-wavelength signatures resident in the signal. The cubic spline methodology, however, fails to fit the short-wavelength signal and noise components within the error signal. This brings into doubt the use of the method for studies that require accuracy at the medium and short wavelengths. However, for our purposes, the procedure is of use since the resulting spline fit to the dual crossover residuals was 5.8 cm RMS over the entire geodetic phase. This represents a significant improvement over the uncorrected RMS dual crossover residuals of 12.11 and 11.39 cm for TOPEX and Poseidon respectively.

All ERS altimetry was corrected using model corrections for solid Earth, CSR3.0 ocean, ocean loading and long period tides (Eanes and Bettadpur 1995), wet tropospheric path delay derived from the ERS-1 microwave sounder, model dry troposphere, Bent model ionospheric path delay and sea-state bias computed as 5.95% of the significant wave height (see Carnochan 1997). A correction for inverse barometer (IB) effect was also computed to reduce variability effects. Additionally, systematic errors caused by drift in the ultra stable oscillator (USO) and bias jumps caused by instrument temperature gradients during switch-off were minimised via corrections supplied by ESRIN. Finally, data were edited if 10-per-second sea height observations had a standard deviation exceeding 25 cm, wet tropospheric corrections were derived from a model, significant wave height exceeded 25 m, backscatter coefficient (σ°) was outside $6 \leq \sigma^\circ \leq 25$ dB and any other model failed to supply a correction.

The corrected data contain a significant aliased variability signal. With altimetric repeat cycles, variability may be effectively reduced by stacking these repeat cycles to produce a data set containing an averaged variability signal. However, with the non-repeating geodetic phase stacking cannot be achieved. Thus any mean sea surface produced will still contain the variability signal. Other MSS models utilising ERS-1 geodetic phase altimetry have suffered from the appearance of ground tracks in regions of large-scale variability. Rapp (1997) suggests that a post-processing correction be applied from the computation of cross-track gradients to alleviate the problem. However, it is more convenient to reduce the variability signal at the pre-processing stage. This was achieved via the computation

of 5-day-interval optimally interpolated variability models from TOPEX altimetry (Lam and Moore 1995) gridded in 2° latitude by $360/127^\circ$ longitude bins.

For MSS recovery, data were sorted into bins of square size 0.075° corresponding to the ERS-1 2×168 -day equatorial ground-track spacing of approximately 8 km. A weighted average for each bin was determined using weights $W_j = e^{-l/\sqrt{2}\Delta x}$ for the j th measurement, where l is the distance from the grid point in degrees and Δx the grid spacing, also in degrees. Additionally, an iterative scheme was employed with a $\pm 3\sigma$ rejection criterion before the new average was computed. For ERS-1, gridded values of d_0 are computed over the whole $\pm 82^\circ$ latitudinal range despite erroneous radial orbit error minimisation outside the TOPEX coverage.

4 The auto-covariance function, $C_{h_0h_0}$

The ACV of the first-guess MSS signal, $(d_0 - h_{lw})$, in Eq. (12) is used here as a signature for errors within the MSS. This function, $C_{h_0h_0}$, was computed from a combination of: EGM96 geoid error degree variances, σ_n^e ; EGM96 geoid degree variances to degree 360, i.e. D_n ; and a geoid degree variance fit, D_n^f , computed to deal with the EGM96 spectral limit for degrees beyond 360.

The ACV function, C_{TT} , of the anomalous geopotential, T , as determined from spherical harmonic expansion, is given by Heiskanen and Moritz (1967) as

$$C_{TT} = \sum_{n=1}^{n_{\max}} \sigma_n^2 P_n(\cos \psi) \quad (15)$$

where n is the degree; $P_n(\cos \psi)$, Legendre polynomials; ψ the spherical distance between two points; and $n_{\max} = 2400$ corresponds to the maximum resolution obtainable. σ_n^2 are potential degree variances calculated from

$$\sigma_n^2 = \sum_{m=0}^n (\sigma_{\bar{C}_{nm}}^2 + \sigma_{\bar{S}_{nm}}^2) \quad (16)$$

where m is the order and $\sigma_{\bar{C}_{nm}}$, $\sigma_{\bar{S}_{nm}}$ are standard deviations of the gravity field harmonics \bar{C}_{nm} and \bar{S}_{nm} respectively. On the geoid the ACV was computed from Brun's equation, $N = T/\gamma$, where N is the geoid height in metres, T the anomalous potential ($\text{m}^2 \text{s}^{-2}$) and γ , the normal gravity (m s^{-2}). Thus, rearranging Eq. (15) to take into account Brun's equation gives the ACV

$$C_{h_0h_0} = R_e^2 \sum_{n=1}^{n_{\max}} \hat{\sigma}_n^2 P_n(\cos \psi) \quad (17)$$

where R_e is the mean radius of the Earth. $\hat{\sigma}_n^2$ represents degree variances for the signature MSS model as developed from

$$\hat{\sigma}_n = \begin{cases} \sigma_n^e, & 2 \leq n \leq 30 \\ D_n, & 31 \leq n \leq 360 \\ D_n^f, & 361 \leq n \leq 2400 \end{cases} \quad (18)$$

where σ_n^e , D_n and D_n^f are standard deviations for EGM96 geoid error, EGM96 geoid and EGM96 geoid extrapolation fit respectively. EGM96 geoid and geoid error degree standard deviations are displayed in Fig. 1.

Figure 2 shows the complete degree standard deviation fit as used to describe the distribution of spherical degree signal energy for the MSS signature. The fit for $n > 360$ was extrapolated to potential degree variances, D_n^f , via $7 \times 10^{-22} n^{-4.55}$. It can also be seen in Fig. 2 that between degrees 2 and 30 an EGM96 model error, σ_n^e , and an error fit, σ_n^{ef} , are provided. In fact the fit σ_n^{ef} is used since the rather large discontinuity at $n = 30$ between σ_n^e and D_n is large enough to cause significant spectral *ringing* with the ACV conversion to the frequency domain. The fit σ_n^{ef} to the EGM96 potential degree variances between degrees 2 and 30 is given by $2.5 \times 10^{-5} n^{-5.1}$.

Given this arrangement, $C_{h_0h_0}$ was calculated using Eq. (17) over the globe at the same grid specifications as previously described (i.e. 0.075°). The spherical angle, ψ , between two points is determined from basic spherical trigonometry (Todhunter and Leathem 1901), as

$$\psi = \cos^{-1}[\cos \phi' \cos \lambda'] \quad (19)$$

where ϕ' and λ' are latitudinal and longitudinal coordinates referenced to a particular computation point. The one-dimensional normalised ACV is shown in Fig. 3 for the EGM96 error, geoid error and reduced MSS signature. These show the various signal correlation lengths provided at the half normalisation point.

The power spectral density, $P_{h_0h_0}$, can be computed using the FFT relationship given in Eq. (6); its perfect symmetry implies that windowing is not required. However, windowing was used to maintain consistency with other parameters. In the spectral domain, $P_{h_0h_0}$ is almost entirely real, with FFT rounding errors resulting in a negligible ($< 10^{-18}$) imaginary component.

5 Altimetric error PSD, P_{nn}

Typically within spatial optimal interpolation, a set of model covariance functions describing the major altimetric error sources would be used. Thus in Wunsch and

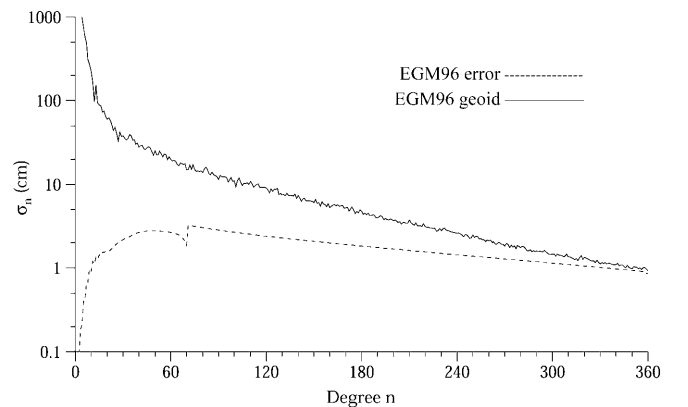


Fig. 1. EGM96 geoid and geoid error degree standard deviations

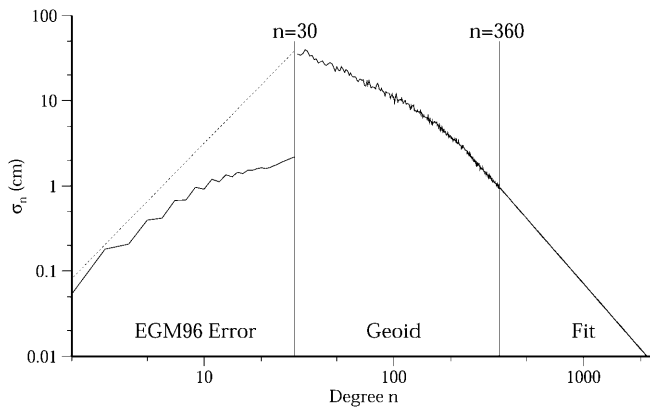


Fig. 2. Degree constructed standard deviations for first guess description of the reduced wavelength MSS. Between degrees 2 and 30 there is the EGM96 geoid error and a linear fit to remove the discontinuity at degree 30 (see text for further explanation)

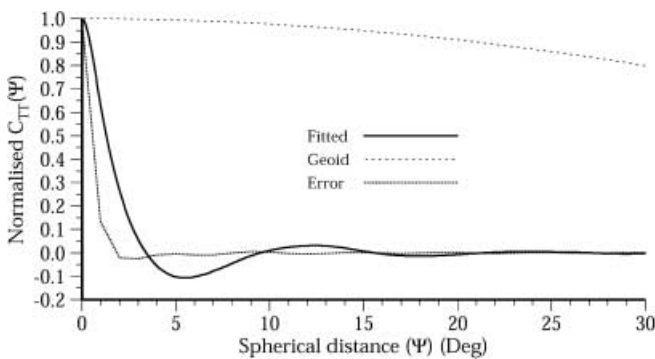


Fig. 3. 1-dimensional auto-covariance function. The three curves are denoted by (a) EGM96 plus the fitted error, (b) EGM96 geoid and (c) EGM96 geoid error

Zlotnicki (1984), Mazzega and Houry (1989) and Blanc et al. (1990) covariance models are computed for the radial orbit, instrumental, atmospheric propagation and oceanic variability errors. From the error sources, a

total error ACV function, C_{nm} , would be obtained. However, due to computational restrictions, studies have been limited to small regions. Unfortunately, at high resolution, global modelling of these covariance parameters is time consuming. Since the PSD of a function may be obtained either from its covariance or from itself, we investigate the use of altimetry to form the PSD of the errors resident within the signal.

The prospect of using altimetry for this is advantageous in terms of computation speed and in not having to rely on model covariances. First of all a residual altimetric surface is computed by removing the sea surface topography, ζ_{20} , and geoid, N_{360} , using Eq. (13) from a first-guess MSS, i.e.

$$S_r(\phi, \lambda) = M(\phi, \lambda) - N_{360}(\phi, \lambda) - \zeta_{20}(\phi, \lambda) \quad (20)$$

where S_r is the residual surface and M the original gridded MSS. Removal of N_{360} from the MSS gives a measure of ERS-1 geodetic phase sea surface topography; see Fig. 4. Further removal of ζ_{20} gives the residual surface, S_r , shown in Fig. 5. A first impression of Fig. 5 reveals that low-amplitude orbit streaks dominate the surface. A closer examination, however, reveals that residual short-wavelength tectonic signatures are also visible. This surface contains degree 2 to 360 EGM96 geoidal error, degree 1 to 20 EGM96 sea surface topography error and errors in all correction parameters (see Sect. 3). Unfortunately, the residual surface also contains MSS signal power for degrees greater than 360; this problem will be dealt with shortly. First, however, some land/ice and water boundary points that result in residual values in excess of 50 cm remain. These points were detected and removed via the use of a Laplacian non-directional edge detection algorithm. The reduced surface was further edited for points outside a threshold limit set at $\pm 3\sigma$; this coped well with the removal of erroneous boundary points.

The residual surface contains large land and ice based regions that cannot easily be filled. However, since the signal and therefore boundary discontinuities are small,

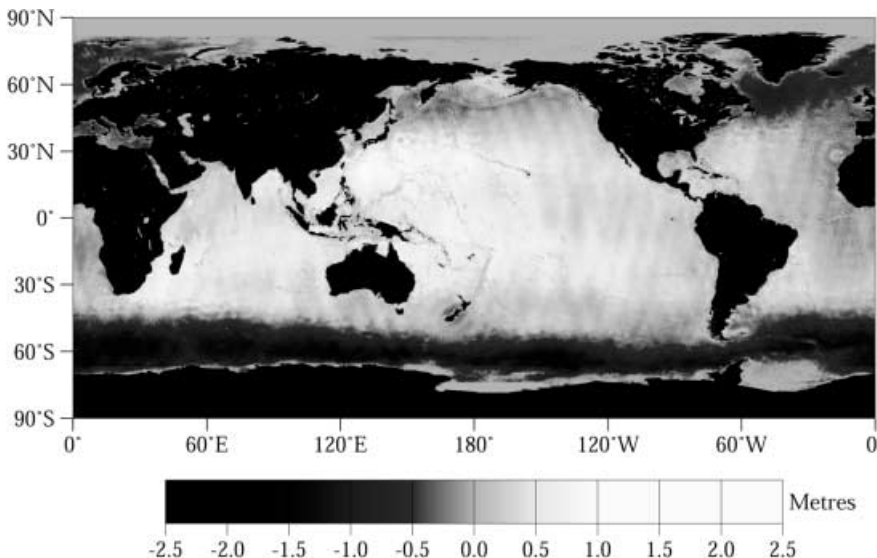


Fig. 4. ERS-1 geodetic phase sea surface topography with RMS value of 0.65 meters

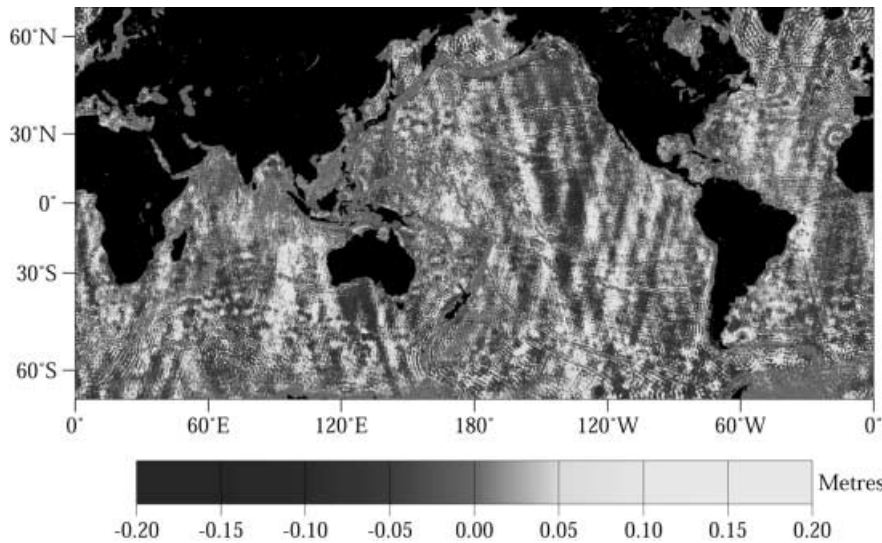


Fig. 5. Residual ERS-1 surface revealing familiar residual orbit error streaks and very small scale (> 360 degrees) tectonic features. The RMS of this surface is 29 cm

the surface was transformed without any filling strategy. The residual signal, S_r , is now converted to its equivalent PSD, P_{S_r} , after appropriate Hanning windowing between latitude degrees 75 and 82. Note that as S_r is non-symmetric, its Fourier domain representation is complex.

As mentioned earlier, removal of EGM96 sea surface topography and geoid results in a complete high-frequency sea surface signal. The final noise spectrum, P_{nm} , may therefore be obtained via a scaling of P_{S_r} above degree $n = 360$, so that

$$P_{nm} = \begin{cases} P_{S_r}, & 2 \leq n \leq 360 \\ P_{S_r}/B, & n > 360 \end{cases} \quad (21)$$

where B represents a scaling factor that was initially given a value of 10. A logarithmic plot of P_{nm} is shown in

Fig. 6. Here the residual radial orbit error is clearly seen as the oval shape surrounding the centre of the figure. Isolation of this feature followed by an inverse transformation regenerated the orbit streaks seen in Fig. 5.

6 Results and validation

After computation of each of the spectral parameters, P_{ss} and P_{nm} , the spectral LS estimator, A_{sl} , may be derived via Eq. (9) through addition and division at each discrete frequency location. The optimally interpolated MSS may then be obtained from Eq. (14). It must be noted that the reduced sea surface grid ($d_0 - h_{lw}$) will contain land regions devoid of data, creating large boundary discontinuities. Since the FFT procedure requires a complete data set, it is necessary to fill void

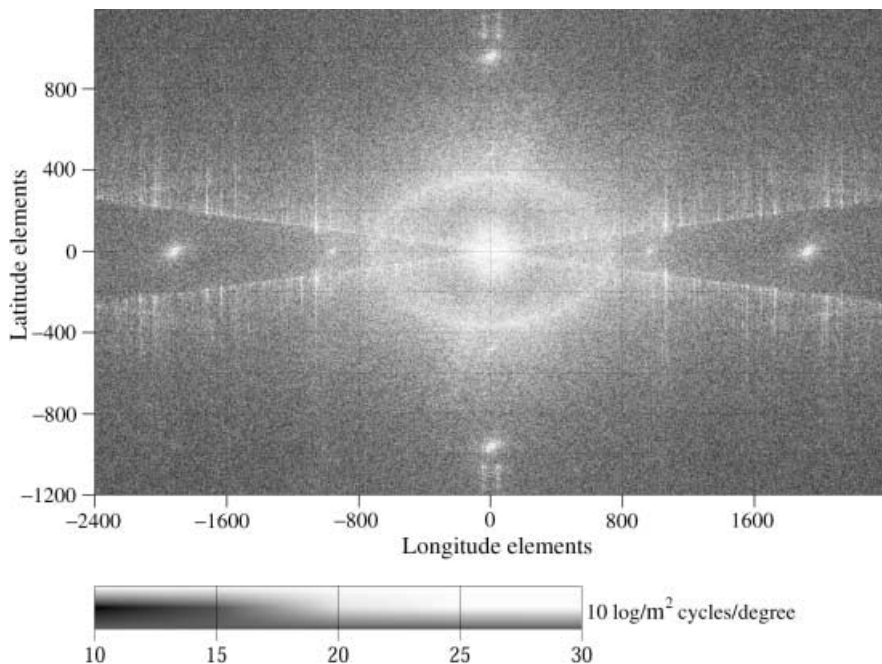


Fig. 6. Spectrum of gridded residual ERS-1 surface

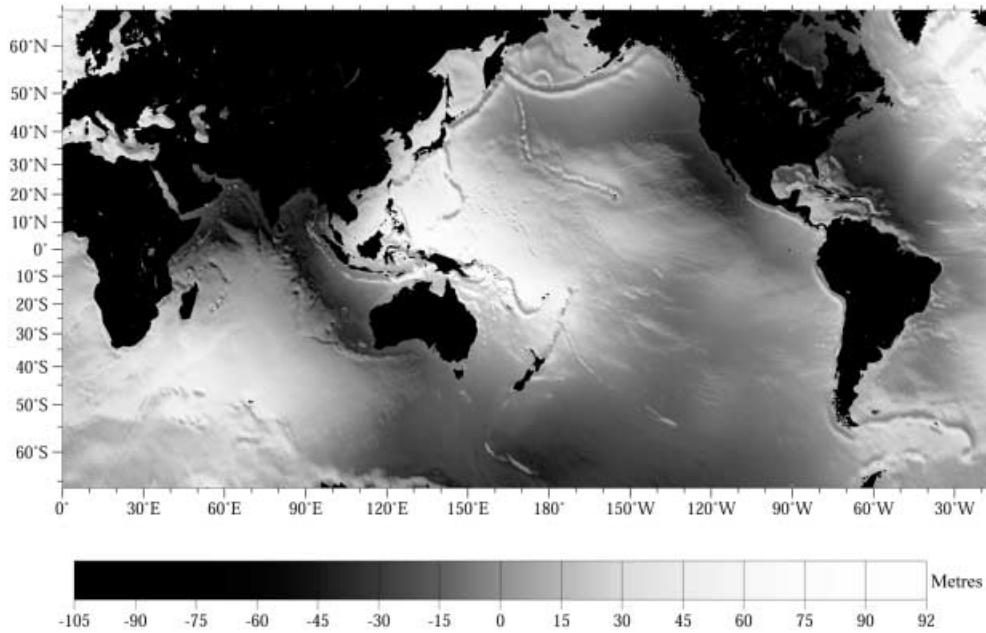


Fig. 7. Global mean sea surface from ERS-1 geodetic phase data using a Mercator projection

regions; here we simply used the EGM96-derived geoid expanded from degree 31 to 360. Additional filtering was conducted by a cosine windowing function between the relevant frequencies to reduce any high-frequency noise. The resultant spectral surface was transformed back to the spatial domain where the long-wavelength EGM96 geoid and sea surface topography were reinstated. The optimally interpolated MSS with a re-established geoid (N_{30}) and sea surface topography (ζ_{20}) is presented in Fig. 7.

As the MSS developed within this paper does not contain direct TOPEX data, and since TOPEX gives the most accurate sea heights to date, it is reasonable to use TOPEX data as an independent means of validating the MSS. There are 33 T/P cycles covering the ERS-1 geo-

detic phase. Fifteen TOPEX cycles were chosen for evaluation, starting with cycle 58 and then every second cycle up to and including cycle 86.

Each TOPEX corrected sea surface height was retrieved and sea surface variability removed by the procedure described in Lam and Moore (1995). The four surrounding MSS grid points were found and a comparison height calculated via bi-linear interpolation. Differences were recorded and rejections made at threshold differences of 60 cm. Table 1 contains the full set of results against TOPEX data. Comparisons are given for shallow water (16.5–18.5 cm RMS), ocean (12.3–13.8 cm RMS) and for all data (12.7–14.1 cm RMS). For the un-optimally interpolated MSS a comparison (also Table 1) for shallow (19.9–20.7 cm RMS),

Table 1. Validation of optimally interpolated MSS against TOPEX altimetry. Comparison is made over shallow water, ocean and both; σ_{oi} and σ_u are RMS values for the optimally interpolated and original surfaces respectively

Cycle No.	Shallow water				Ocean				Ocean and shallow			
	No. of points	No. of rejections	σ_{oi} (cm)	σ_u (cm)	No. of points	No. of rejections	σ_{oi} (cm)	σ_u (cm)	No. of points	No. of rejections	σ_{oi} (cm)	σ_u (cm)
58	37 978	5876	17.9	20.6	466 854	19 051	13.5	16.0	504 832	24 927	13.8	16.3
60	38 870	6108	17.4	20.1	456 290	14 363	13.5	15.9	495 159	20 471	13.8	16.3
62	40 635	6873	18.1	20.5	449 658	12 040	13.3	15.7	490 293	18 913	13.6	15.8
64	41 919	7038	17.6	20.3	440 646	9991	13.0	15.8	482 565	17 029	13.4	16.2
66	42 959	7534	16.5	19.9	433 848	8855	12.3	15.7	476 807	16 385	12.7	16.1
68	43 721	8141	17.7	20.2	424 169	7999	12.9	15.7	467 890	16 140	13.3	16.1
70	46 456	9169	17.9	20.3	423 010	7729	13.3	15.8	469 466	16 898	13.7	16.2
72	48 632	9608	17.7	20.7	419 016	7516	13.4	15.9	467 648	17 124	13.9	16.3
74	49 552	10 145	18.5	20.5	419 456	7707	13.7	15.7	469 008	17 852	14.1	16.2
76	48 465	9913	18.3	20.5	415 101	7613	13.7	15.9	463 566	17 526	14.1	16.3
78	48 660	9653	18.2	20.2	422 631	7615	13.6	15.8	471 291	17 268	14.0	16.2
80	45 536	8625	18.0	20.4	423 357	8225	13.6	15.9	468 893	16 850	13.9	16.3
82	42 306	6913	18.4	20.2	439 551	10 553	13.7	16.1	481 857	17 466	14.0	16.4
84	39 316	6076	17.9	20.6	456 689	15 010	13.8	16.2	496 005	21 086	14.1	16.5
86	37 802	6059	18.3	20.6	463 180	18 166	13.8	16.1	500 982	24 225	14.1	16.5

ocean (15.7–16.2 cm RMS) and all data (15.8–16.5 cm RMS) was also made. An improvement of the spectrally optimally interpolated MSS over the original has thus been made at the 3–4-cm RMS range over all ocean types. This is equivalent to a near 10-cm improvement in heights assuming a normal distribution for the refinement. An example of global comparisons between the optimally and un-optimally interpolated surfaces is given in Fig. 8 for cycle 66. Here, an overall reduction in differences is evident between the two surfaces.

A comparison has been made with the original ERS-1 altimeter geodetic phase data. The altimetry was corrected for geophysical effects with radial orbit error and sea surface variability reduced by the aforementioned

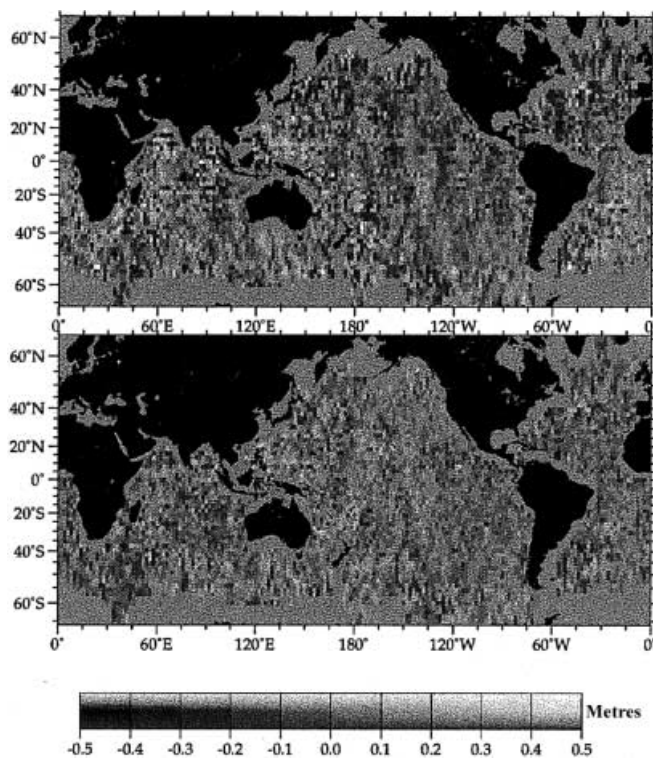


Fig. 8. Comparison of the mean sea surface against TOPEX cycle 66 sea surface heights (top) before optimal interpolation and (bottom) after optimal interpolation

procedures. The data was split into nine sub-cycles of 37 days and a comparison made as summarised in Table 2. Here differences are between 10.1 and 10.3 cm RMS over all cycles against approximately 14.5 cm RMS for the un-optimally interpolated surface. Against enhanced GEOSAT sea heights (see Table 3), the model provided a poorer fit. However, considering the mis-modelling within GEOSAT altimetry (i.e. orbital accuracy and lack of radiometer), the results are reasonably good. Comparisons reveal a model fit of approximately 18 cm RMS against approximately 22 cm for an un-optimally interpolated surface.

For completeness, a comparison was made with the OSU-95 MSS obtained from the TOPEX GDR with an RMS difference of 15.1 cm between the two surfaces. Also of interest are comparisons of the TOPEX cycles against EGM96 and OSU91A. The EGM96 geoid plus sea surface topography model gave an RMS of 26.5–27.5 cm, whilst for the OSU91A it was approximately 29 cm, thus confirming the improvement between these two models.

7 Conclusions

The theory and practical methodology used to determine a high-resolution/precision MSS model has been described. In summary the procedure is as follows: (1) minimisation of radial orbit error via the use of a modified Le Traon et al. cubic spline fitting to dual ERS-1 and TOPEX crossovers; (2) removal of TOPEX-derived sea surface variability in order to reduce cross-track gradients in the end product; (3) gridding of the ERS-1 geodetic phase altimetric data set; and (4) spectral optimal interpolation, including the generation of several geophysical parameters followed by inverse transformation.

In comparison, recent MSS models, such as those described by Kim (1993), Yi (1995) and Cazenave et al. (1995), show differences with T/P in the region of 9.5–13 cm RMS. All these models, however, contain a years' worth of TOPEX data and therefore have an advantage when compared against the same data. Thus, although such models may be good along-track, there is no actual means of assessing the performance off the T/P ground

Table 2. Optimally interpolated and un-optimally interpolated MSS against nine sub-cycles of ERS-1 geodetic phase altimetry

Cycle no.	Shallow water				Ocean				Ocean and shallow			
	No. of points	No. of rejections	σ_{oi} (cm)	σ_u (cm)	No. of points	No. of rejections	σ_{oi} (cm)	σ_u (cm)	No. of points	No. of rejections	σ_{oi} (cm)	σ_u (cm)
1	119 077	8075	16.9	19.8	1 427 378	19 983	9.3	14.1	1 546 455	38 058	10.0	14.6
2	123 960	18 817	16.8	19.9	1 423 606	19 930	9.4	14.0	1 547 566	38 747	10.1	14.5
3	118 936	18 054	17.1	20.3	1 365 908	17 756	9.3	14.1	1 484 844	35 810	10.0	14.6
4	129 162	19 606	17.3	20.2	1 406 652	18 286	9.5	14.3	1 535 814	37 892	10.3	14.8
5	129 549	19 665	17.2	20.1	1 407 212	18 293	9.6	14.2	1 536 761	37 958	10.3	14.7
6	128 989	19 503	17.0	20.3	1 415 789	19 821	9.5	14.2	1 544 778	39 324	10.2	14.7
7	128 569	19 516	17.1	20.1	1 426 074	19 965	9.4	14.1	1 554 643	39 481	10.2	14.6
8	136 218	20 677	16.9	20.2	1 499 052	19 487	9.4	14.0	1 635 270	40 164	10.1	14.5
9	179 127	27 191	16.8	20.1	1 928 250	25 067	9.4	13.9	2 107 377	52 258	10.1	14.4

Table 3. Optimally interpolated and un-optimally interpolated MSS against ten 23-day sub-cycles of GEOSAT geodetic mission altimetry

Cycle no.	Shallow water				Ocean				Ocean and shallow			
	No. of points	No. of rejections	σ_{oi} (cm)	σ_u (cm)	No. of points	No. of rejections	σ_{oi} (cm)	σ_u (cm)	No. of points	No. of rejections	σ_{oi} (cm)	σ_u (cm)
1	142 469	23 899	21.3	29.1	834 650	70 889	18.1	21.8	977 119	94 788	18.6	23.0
3	140 209	21 782	20.6	28.7	787 400	54 800	18.1	21.7	927 609	76 582	18.4	22.9
5	152 311	25 695	20.4	28.6	816 324	47 469	17.3	20.6	968 635	73 164	17.8	22.0
7	127 765	22 988	20.5	28.9	712 288	39 193	17.4	20.5	840 083	62 181	17.9	21.9
9	141 123	25 339	20.6	29.4	796 941	43 298	17.2	20.3	938 064	68 637	17.7	21.9
11	142 695	25 674	20.9	29.3	799 649	47 695	17.8	21.0	942 344	73 369	18.2	22.4
13	150 149	29 291	21.3	30.1	868 745	71 320	17.7	21.2	868 745	100 611	18.2	22.7
15	135 992	26 459	21.4	30.1	820 440	75 784	18.8	22.4	956 432	102 243	19.1	23.5
17	126 827	22 067	21.0	29.3	768 265	68 457	17.8	21.5	895 092	90 524	18.4	22.4
19	137 735	22 996	21.3	29.0	722 095	52 779	18.1	21.5	859 830	75 775	18.6	22.9
21	126 370	21 870	21.0	29.1	653 579	41 094	18.1	21.5	779 949	62 964	18.6	22.9
23	104 340	21 091	20.3	29.2	610 020	34 624	17.5	20.5	714 360	55 715	17.9	21.9

track. Inclusion of stacked TOPEX 10-day and ERS-1/2 35-day repeat altimetry into the model described here would almost certainly yield further improvements, as would the inclusion of further refined ERS-1 orbital ephemerides as they become available. However, correct weighting of the TOPEX SSHs is critical as too high a weight will simply give an incorrect assessment of accuracy. The inclusion of ERS-1/2 35-day repeat data would require inter-phase relative biases between ERS-1/2 and TOPEX being dealt with as outlined in Moore et al. (1999).

Clearly the $\pm 66^\circ$ limit to the model presented here is a result of the nature of ERS-1 altimetry being degraded as a result of poor orbit outside these latitudinal limits. Inclusion of stacked ERS-2 altimetry would allow the model to be extended to 82° in the Arctic, although sea-ice contamination is a major concern (see Peacock 1998). However, since the ocean sampling characteristics for the ERS-2 35-day repeat period are different to the ERS-1 geodetic phase a modification would be required to the algorithm.

The proposed launch of CryoSat in 2003 will provide a major contribution to the determination of MSS models over sea-ice surfaces even though it is not a primary scientific goal of the mission (an overview of the mission is given by Wingham 1999). The platform's high inclination, 92° , and long repeat period at 369 days with 5334 revolutions/cycle, results in a very dense ground-track pattern that ideally suits the proposed method defined in this paper. If the secondary objective of an ocean product is given the go-ahead then we will have a unique opportunity to resolve an MSS model in combination with several other data sets on a global scale with improved accuracy.

The inclusion of the IB correction gives some cause for concern since it can cause some side effects despite reducing overall variability (see Yi 1995). This study employed the correction with the overall intention of removing the variability. Quite clearly it would be necessary to examine the effect without the inclusion of the IB correction. On the subject of variability, the authors made it a special case to remove variability derived from TOPEX data, as described in Sect. 3 during pre-

processing of the altimetry. The fixed-resolution grids used cannot assist in the removal of variability at the higher resolution of the MSS model. It therefore remains to be seen what the overall effect of the remaining higher-frequency components of variability is. Further analysis is therefore required.

A study to refine B [Eq. (21)] via an iterative process would be expected to yield a minor improvement in the final surface with the a posteriori covariance given in Eq. (11) being used to assess any improvement. It also remains to be seen whether the removal of the EGM96 geoid model to degree and order 30 needs to be fixed at this value. A re-assessment of the problem may allow the removal of the complete model. Finally, a further examination of how the altimetric error surface compares with model covariances describing the altimetric error would be useful. Here, covariances determined empirically from the altimetry could help improve modelling, and vice versa.

Acknowledgements. The authors would like to thank the UK Natural Environment Research Council (Grant No. GT12/94/66/D) for financing this study. They would also like to thank the reviewers for their constructive comments and suggestions.

References

- Anzenhofer M, Gruber T (1995) MSS93A: a new stationary sea surface combining one year up-graded ERS-1 fast delivery data and 1987 Geosat altimeter data. *Bull Géod* 69: 157–163
- AVISO (1996) Archiving, validation and interpretation of satellite oceanography, AVISO handbook for merged TOPEX–Poseidon products, 3rd edn, AVI-NT-02-101-CN. AVISO, Toulouse
- Blanc F, Houry S, Mazzega P, Minster JF (1990) High resolution, high accuracy altimeter derived mean sea surface in the Norwegian sea. *Mar Geod* 14: 57–76
- CERSAT (1994) Centre ERS d'Archivage et de Tractement, CI-EX-MUT-A21-01-CN Centre Ifremer, BP 70, 29280 Plouzane, France
- Carnochan S (1997) Altimeter and orbit corrections for the ERS satellites through the analysis of single and dual satellite crossovers. PhD thesis, University of Aston, Birmingham, UK
- Carnochan S, Moore P, Ehlers S, Lam C, Woodworth P (1994) Improvement of radial positioning of ERS-1 through dual crossover analysis with TOPEX–Poseidon. SP 361, European Space Agency

- Cazenave A (1994) The geoid and oceanic lithosphere. In: Vaniček P, Christou, NT (eds) *Geoid and its geophysical interpretations*, Chap. 13. CRC Press, Boca Raton, pp 255–283
- Cazenave A, Parsons B, Calcagno P (1995) Geoid lineations of 1000 km wavelength over the Central Pacific. *Geophys J Int* 22(2): 97–100
- Cazenave A, Schaeffa P, Berge M, Brossier C, Dominh K, Gennero MC (1996) High-resolution mean sea surface computed with altimeter data of ERS-1 (geodetic mission) and TOPEX–Poseidon. *Geophys J Int* 125: 696–704
- Cullen R (1998) Mean sea surface modelling from multi-satellite radar altimetry utilising Fourier domain techniques. PhD thesis, University of Aston, Birmingham, UK
- Dickey JO, Bentley CR, Bilham R, Carton JA, Eanes RJ, Herring TA, Kaula WM, Lagerloef GSE, Rojstaczer S, Smith WHF, van den Dool HM, Wahr JM, Zuber MT (1998) Satellite gravity: insights into the solid Earth and its fluid envelope. *EOS Trans AGU* 79(20): 237–248
- Eanes RJ, Bettadpur SV (1995) The CSR3.0 global ocean tide model. Tech rep CSR-TM-95-06, Centre for Space Research, University of Texas at Austin
- Heiskanen WA, Moritz H (1967) *Physical geodesy*. WH Freeman, San Francisco
- Jolly GW, Moore P (1996) Analysis of global ERS-1 altimetry by optimal Fourier transform interpolation. *Mar Geod* 19: 331–357
- Kim MC (1993) Determination of high resolution mean sea surface and marine gravity field using satellite altimetry. PhD thesis, University of Texas at Austin
- Knudsen P (1999) A global high resolution mean sea surface from multi mission satellite altimetry. *Phys Chem Earth* 24(4): 407–409
- Lam CW, Moore P (1995) A study of sea surface variability in the southern oceans using ERS-1 altimetry. In: Curran PJ, Robertson C (eds) *RSS 95 – Remote sensing in action*. Proc 21st Ann Conf Remote Sensing Society, University of Southampton, pp 78–85
- Le Traon P, Gaspar P, Bouyssel F, Makhmaraa H (1995) Use of TOPEX–Poseidon data to enhance ERS-1 data. *J Atmos Ocean Technol* 12: 161–170
- Lemoine FG, Smith DE, Kunz L, Smith R, Pavlis EC, Pavlis NK, Klosko SM, Chinn DS, Torrence MH, Williamson RG, Cox CM, Rachlin KE, Yang YM, Kenyon SC, Salman R, Trimmer R, Rapp RH, Nerem RS (1996) The development of the NASA GSFC and NIMA joint geopotential model. Proc Int Symp Gravity, Geoid, and Marine Geodesy (GRANGEOMAR 1996), Tokyo, 30 Sept–5 Oct. Springer, Berlin Heidelberg New York
- Mazzega P, Houry S (1989) An experiment to invert Seasat altimetry for Mediterranean and Black Sea mean surfaces. *Geophys J* 96: 259–272
- Moore P, Carnochan S, Walmsley RJ (1999) Stability of ERS altimetry during the tandem mission. *Geophys Res Lett* 26(3): 373–376
- Moritz H (1980) *Advanced physical geodesy*. H. Wichmann, Heidelberg
- Peacock NR (1998) Arctic sea ice and ocean topography from satellite altimetry. PhD thesis, University of London
- Rapp R, Yuchan Y, Wang YM (1994) Mean sea surface and geoid gradient comparisons with TOPEX altimeter data. *J Geophys Res* 89: 24 657–24 667
- Rapp RH (1997) Mean sea surface used for the Geosat JGM-3 GDRs. Geosat online handbook at: <http://www.nodc.noaa.gov/NODC-cdrom>
- Rapp RH, Nerem RS (1995) Geoid undulation and mean sea surface recommendations. Paper presented at the TOPEX–Poseidon Science Working Team Meeting, Jet Propulsion Laboratory, Pasadena
- Schwarz KP, Sideris MP, Forsberg R (1990) The use of FFT techniques in physical geodesy. *Geophys J Int* 100: 485–514
- Tapley BD, Watkins MM, Ries JC, Davis GW, Eanes RJ, Poole SR, Rim HJ, Schutz BE, Shum CK, Nerem RS, Lerch FJ, Marshall JA, Klosko SM, Pavlis NK, Williamson RG (1996) The joint gravity model 3. *J Geophys Res* 101(B12): 28 029–28 049
- Todhunter I, Leathem JG (1901) *Spherical trigonometry*. MacMillan, London
- Wang YM (2000) The satellite altimeter data derived mean sea surface GSFC98. *Geophys Res Lett* 27(5): 701–704
- Wingham DJ (1999) The first of ESA's first opportunity missions: CryoSat. *Earth Observ Quart* 63: 21–24
- Wunsch C, Zlotnicki V (1984) The accuracy of altimetric surfaces. *Geophys J Roy Astron Soc* 78: 795–808
- Yi Y (1995) Determination of gridded mean sea surface from TOPEX, ERS-1 and GEOSAT altimetry data. Rep 434, Department of Geodetic Science and Surveying, The Ohio State University, Columbus